

Review of Mesoscale Geometric Models of Concrete Materials

Jiajun Zhang ¹, Rujin Ma ^{1,*} , Zichao Pan ¹ and Haijun Zhou ² 

¹ College of Civil Engineering, Tongji University, Shanghai 200092, China; 2310100@tongji.edu.cn (J.Z.); z.pan@tongji.edu.cn (Z.P.)

² College of Civil and Transportation Engineering, Shenzhen University, Shenzhen 518060, China; haijun@szu.edu.cn

* Correspondence: rjma@tongji.edu.cn

Abstract: Concrete can be regarded as a composite material comprising aggregates, cement mortar, and an interfacial transition zone (ITZ) at the mesoscale. The mechanical properties and durability of concrete are influenced by the properties of these three phases. The establishment of a mesoscale model of concrete and the execution of numerical simulations constitute an efficacious research method. It is an efficacious method to research concrete by establishing the mesoscale model of concrete and executing numerical simulations. By this method, the influence of an aggregate shape on concrete performance can be studied. This paper presents a systematic review of mesoscale modeling methods for concrete, with a focus on three aspects: the aggregate modeling method, the collision detection algorithm, and the particle-packing algorithm. The principal processes, advantages, and disadvantages of various methods are discussed for each aspect. The paper concludes by highlighting current challenges in the mesoscale modeling of concrete.

Keywords: concrete; aggregate; meso-modeling; contact detection; particle-packing algorithms



Citation: Zhang, J.; Ma, R.; Pan, Z.; Zhou, H. Review of Mesoscale Geometric Models of Concrete Materials. *Buildings* **2023**, *13*, 2428. <https://doi.org/10.3390/buildings13102428>

Academic Editor: Binsheng (Ben) Zhang

Received: 26 July 2023

Revised: 20 September 2023

Accepted: 21 September 2023

Published: 23 September 2023



Copyright: © 2023 by the authors. Licensee MDPI, Basel, Switzerland. This article is an open access article distributed under the terms and conditions of the Creative Commons Attribution (CC BY) license (<https://creativecommons.org/licenses/by/4.0/>).

1. Introduction

Concrete is the most widely used construction material and has been extensively studied at the macroscale, mesoscale, and microscale [1]. The choice of scale depends on the research question being addressed. At the macroscale, concrete is treated as a homogeneous material. At the mesoscale, it is considered a composite material composed of aggregate, cement paste, and the ITZ between them [2]. The ITZ is a special microstructure that forms on the surface of aggregates, and its thickness is influenced by factors such as cement particle size and curing conditions [3]. At the microscale, cement paste is composed of unhydrated cement particles, hydration products, and capillary pores. The key to establishing a mesoscale model of concrete is to accurately simulate the shape and distribution of aggregates within the cement paste. The mechanical properties of concrete [4–7] and the transport of aggressive agents within the cement paste are affected by the shape and distribution of aggregates [8–10], which makes the development of a realistic mesoscale model an important step in numerical simulations.

In 1983, Wittmann [11] defined the three structural levels of concrete and introduced the multi-scale method to study concrete. At the mesoscale, Bažant et al. [12], and Zubelewicz and Bažant [13] used the random particle model to study the fracture of concrete, and Vonk [14] used the regular hexagon build concrete model at the mesoscale to study the softening of concrete loaded in compression. After that, researchers combined mesoscale geometric models of concrete with different simulation methods to study the performance of concrete. A common simulation method is the lattice model. Cusatis et al. [15,16] used the lattice model to study the failure behavior of concrete at the mesoscale. Schlangen and Garboczi [17], and Lilliu and van Mier [18] combined the lattice model with the mesoscale model of concrete to analyze the fracture of concrete materials. In addition, the mesoscale model of concrete is often combined with zero-thickness finite elements [19], the rigid spring block method [20,21], and the discrete element method [22–24].

From the perspective of the research object, the mesoscale model of concrete has been widely applied to study the mechanical performance [25] and durability of concrete [26–31], including crack initiation and propagation, and chloride-induced degradation. Jin et al. [32] proposed the law of static and dynamic uniform size effects by building mesoscale models of concrete. Pedersen et al. [5] used a 2D mesoscale model, and its accuracy was verified by experimental data [33,34], to predict the dynamic tensile behavior of concrete with varying saturation. Ma et al. [35] developed a mesoscale model of concrete with random aggregates to study the flexural failure process of fully graded concrete. Furthermore, mesoscale models are also important to study concrete durability [36]. The transport of chemical agents within concrete can be affected by the impermeability of aggregates, resulting in a tortuosity effect [8]. This effect is largely influenced by the shape and distribution of aggregates, making mesoscale modeling an important tool for studying the durability of concrete. Pan et al. [37] developed a stochastic aggregate model with ellipses and polygons to study the spatial variability of chloride caused by the heterogeneity of concrete at the mesoscale. Li et al. [38] developed a mesoscale model of concrete to simulate the diffusion of chloride in freeze–thaw cycles. They verified the accuracy of the multi-scale study of chloride erosion and found that freeze–thaw cycling can accelerate chloride erosion. Numerous studies have demonstrated that the accuracy of numerical simulations can be significantly affected by the mesoscale model of concrete [4–10].

The mesoscale modeling of concrete can be primarily divided into three components: the aggregate modeling method, the collision detection algorithm, and the particle-packing algorithm. The aggregate modeling method is used to characterize the geometry of aggregates. The collision detection algorithm is used to detect whether aggregates are overlapped and obtain collision information. It should be highlighted that the collision algorithm is closely related to the aggregate modeling method. In other words, a corresponding collision algorithm follows the aggregate modeling method. The particle-packing algorithm is used to pack aggregates into the concrete. It is crucial to choose a reasonable method to improve the efficiency and accuracy of the mesoscale model of concrete.

This paper provides a state-of-the-art review of the methods used to model concrete at the mesoscale scale. The main topics include the aggregate modeling method, the collision detection algorithm, the particle-packing algorithm, and specific techniques for modeling concrete at the mesoscale. This paper will introduce the development history of the mesoscale model of concrete modeling, analyze the advantages and disadvantages of commonly used modeling methods, and finally discuss the challenges and possible solutions to aggregate modeling methods.

2. Complex Aggregate Shape Modeling Method

The first stage of conducting a mesoscale model of concrete is the creation of an aggregate model. The shape of the aggregate will affect the mesoscale model of concrete [39]. This section provides a comprehensive introduction and evaluation of the aggregate modeling method. In this section, an aggregate modeling method is evaluated from the following aspects: accuracy, applicability, storage space, and efficiency of modeling. Five types of aggregate modeling methods have been reported in the relevant research: virtual space method, polygonal polyhedron methods, continuous function methods, discrete function methods, and combined particle methods. These methods are discussed in greater detail in this section.

2.1. Virtual Space Method

The virtual space method was first proposed by Jia and Williams [40] for particles of arbitrary shapes. By drawing computer graphics, particles of arbitrary shapes are represented as a collection of discrete voxels as depicted in Figure 1a. If the internal structure of the particles is not taken into consideration, the model can be further simplified by retaining only the voxels on the surface of the aggregate as shown in Figure 1b.

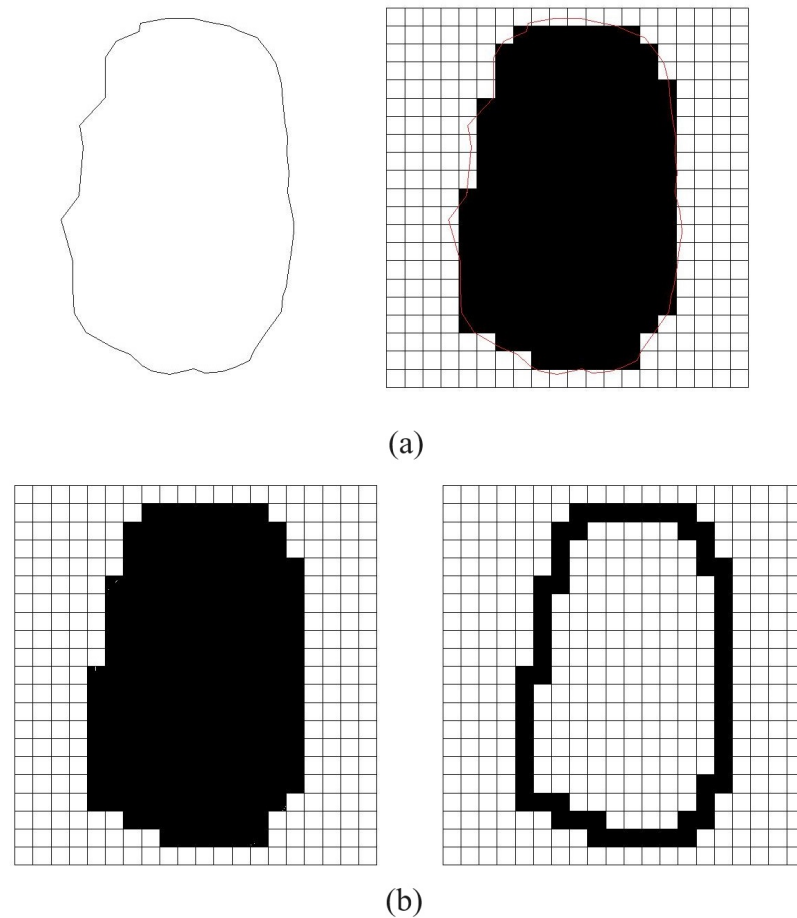


Figure 1. (a) Digitization of a real object. The grid or resolution is usually the compromise between the accuracy required and the computational cost involved. (b) Only the outline of a solid object is actually needed when moving it around and detecting overlaps it may have with others. This dramatically increases the speed of the packing algorithm [40].

For translation, particles are allowed to move within spatial grids with integer cells. For the rotation, the aggregate model based on voxels will potentially result in the creation of voids within the aggregate as depicted in Figure 2. Byholm et al. [41] optimized the calculation of particle voxel model rotation, thereby enhancing computational efficiency and presenting methodologies for resolving the issue of void formation within aggregates.

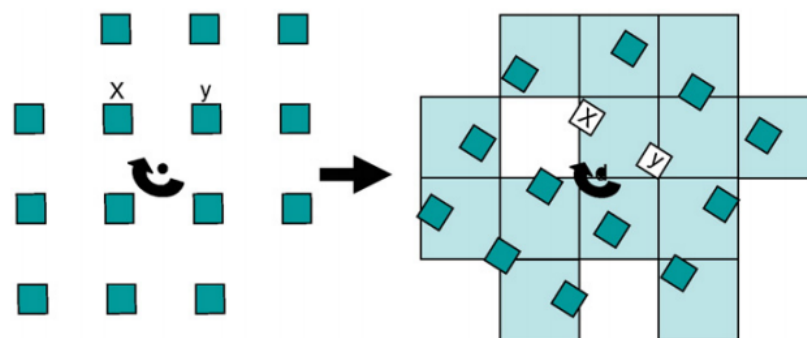


Figure 2. Voxels, exemplified by the two neighboring voxels named *x* and *y*, are rotated into their new positions, resulting in a hole in the structure denoted by the white square. The smaller squares illustrate the voxels being rotated, and the larger squares the resulting positions [41].

The virtual space method has been widely used in the numerical simulation of concrete. Research findings have consistently demonstrated that the shape and orientation of aggregates play a crucial role in determining the properties of concrete [42,43].

The virtual space method shows excellent applicability in modeling aggregates with arbitrary shapes. Jia and Williams [40] used the virtual space method to model aggregates with regular shapes, such as circles, ellipses, and short fibers. This method was further extended to 3D to build aggregates with spheres and ellipsoids [44,45]. Recently, new techniques, such as X-ray CT and laser scanners, have been used to model real aggregates [9,46].

However, it is important to acknowledge that virtual space methods have certain limitations. The accuracy of such methods depends on the voxel resolution employed [47]. The process of voxelization will decrease the accuracy of the aggregates model. The increasing resolution will improve the accuracy of the model, but it also requires larger storage space and thus results in lower modeling efficiency [41].

2.2. Polygon Polyhedron Method

Ghaboussi and Barbosa [48] introduced a methodology for particle modeling known as the polygon polyhedron method. This method involves representing particles using polyhedrons. To define a polygon polyhedron, the coordinates of all vertices are first determined, and then the vertices that make up each face are identified. Additionally, if needed, the normal vector of each face is defined to establish the direction of the face. It should be highlighted that the numbers of faces and vertexes are limited. When the numbers of faces and vertexes are huge, the aggregate modeling method is more suitable for the discrete particle method.

The polygon polyhedron method has been widely used in crushed-stone modeling. Kruggel-Emden and Oschmann [49] used this method to model cubes, pyramids, plates, and icosahedrons. Zhao et al. [50] proposed a method by finding the vertexes on the surface uniformly to generate polyhedrons. Höhner et al. [51] inscribed a sphere at each vertex to smooth the polyhedron, as Figure 3 shows below.

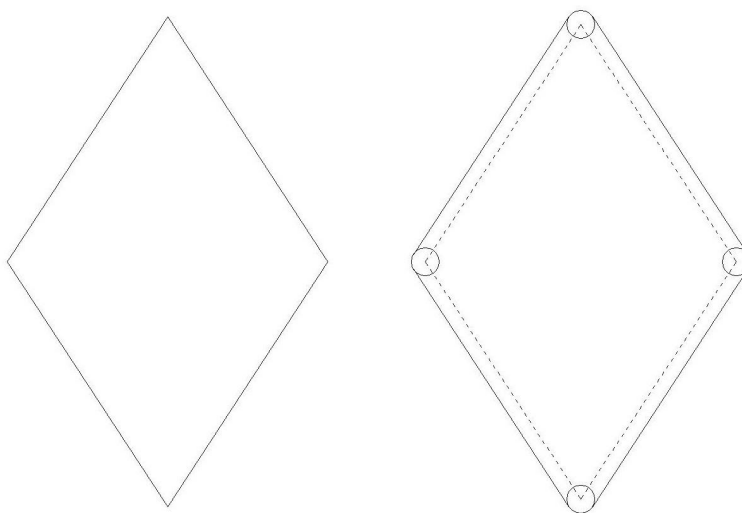


Figure 3. A 2D sketch of a cube (left) and its smoothed polyhedral [51].

The polygonal polyhedron method offers a straightforward modeling method that requires minimal calculation time. Therefore, this method has been widely used [52,53]. However, this method can only be used to model polygon polyhedrons, and its effectiveness in modeling pebbles and aggregates with real shapes is poor.

2.3. Continuous Function Method

The continuous function method characterized the shape of aggregates by employing surface functions. Various shapes are commonly expressed using continuous functions, in-

cluding circles [54], ellipses [55,56], two-dimensional hyper-quadratic curves, spheres [57], ellipsoids, and three-dimensional hyper-quadratic surfaces. Figure 4 displays the two-dimensional hyper-quadratic curves and three-dimensional hyper-quadratic surfaces calculated according to Equations (1) and (2) [58] below:

$$f(x, y) = \left(\frac{x}{a}\right)^{e_1} + \left(\frac{y}{b}\right)^{e_2} - 1 \tag{1}$$

$$f(x, y, z) = \left(\left(\frac{x}{a_1}\right)^{\frac{2}{e_2}} + \left(\frac{y}{a_1}\right)^{\frac{2}{e_2}}\right)^{\frac{e_2}{e_1}} + \left(\frac{z}{a_3}\right)^{\frac{2}{e_2}} - 1 \tag{2}$$

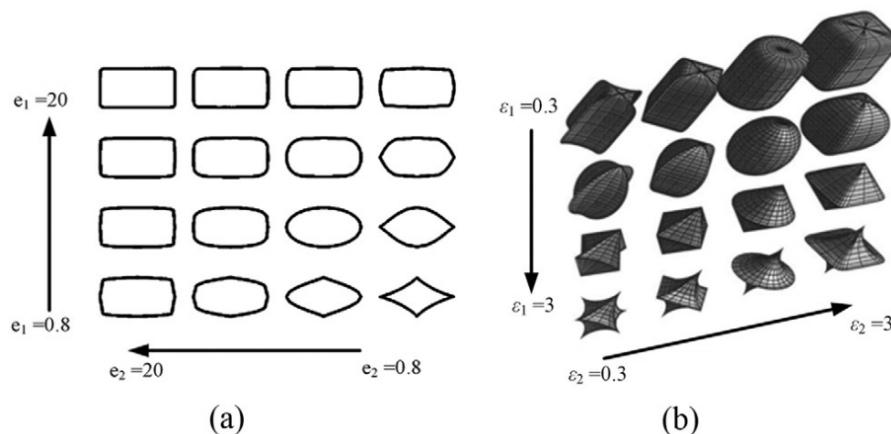


Figure 4. Continuous functions representations [58]: (a) two-dimensional superquadratics; (b) three-dimensional superellipsoids.

To create aggregate models based on real aggregates, researchers have integrated Fourier functions into the continuous function modeling approach within the two-dimensional domain [59,60]. By employing techniques like laser scanning, aggregate surface information can be obtained. By Fourier functions, aggregate surface information can be used to build an aggregate model, and the shape characteristics of aggregate can also be analyzed [61,62]. The equation for the aggregate surface based on Fourier functions is presented as Equation (3):

$$R(\theta) = \sum_{j=0}^{\infty} [a_j \cos(j\theta) + b_j \sin(j\theta)] \tag{3}$$

Garboczi [63], and Garboczi and Bullard [64] expanded upon the continuous function modeling approach by incorporating spherical harmonic functions into the three-dimensional domain. Bullard and Garboczi [65] derived the formulas to calculate aggregate characteristic parameters, including volume and surface area, based on spherical harmonic functions. The equations for the aggregate surface utilizing spherical harmonic functions are presented as Equations (4) and (5):

$$r(\theta, \phi) = \sum_{n=0}^{\infty} \sum_{m=-n}^n a_{nm} Y_n^m(\theta, \phi) \tag{4}$$

$$Y_n^m(\theta, \phi) = \sqrt{\left(\frac{(2n+1)(n-m)!}{4\pi(n+m)!}\right)} P_n^m(\cos(\theta)) e^{im\phi} \tag{5}$$

The modeling of star-shaped aggregates can be effectively achieved by employing Fourier functions and spherical harmonic functions. A star-shaped aggregate is rigorously defined as an aggregate wherein any line segment connecting a point on its surface to the centroid intersects the surface precisely at a single point. Consequently, it is imperative that the aggregate remains free from cavities or overhangs.

While many studies have employed spherical or ellipsoidal equations to model aggregates, research on modeling complex-shaped particles using continuous function methods is still limited. The process of modeling real aggregates remains relatively complex. Modeling aggregates using the Fourier function and spherical harmonic functions allows for the creation of aggregate models of any shape. The obtained models are presented in function form, facilitating model preservation by storing function coefficients, which require minimal storage space.

2.4. Discrete Function Method

Cundall and Strack [66] initially introduced discrete elements as a means to model particle shapes. Building upon this concept, Williams and O'Connor [67] proposed the discrete function method, which involves unfolding the aggregate surface and uniformly selecting discrete points along the X-axis to discretize the aggregate surface function as shown in Figure 5. For three-dimensional particles, there are two types of discrete functions. The first type is a uniform discretization method that can be applied to particles of any shape. It discretizes the aggregate function based on the angles θ_m and ϕ_m in the spherical coordinate system. The second type is an adaptive discretization method specifically designed for superquadratic particles as introduced by Hogue [58]. This method allows for the densification of discrete points at sharp vertices or corners. It ensures that the discretization captures the intricate details of the particles' surfaces. X-ray CT and 3D optical scanner are also used to obtain the discrete points [68].

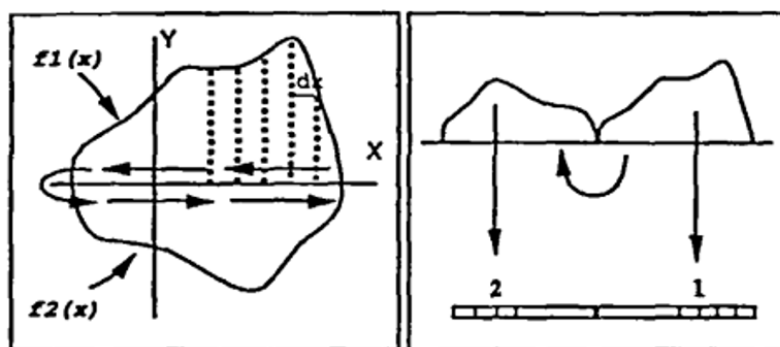


Figure 5. A discretized representation of a single-valued boundary function $y = f(x)$ [67].

Modeling aggregates using the discrete function method can lead to higher accuracy of the model. Therefore, discrete function methods are widely used [69], but they also take up more storage space and computing time. A GPU-based discrete element modeling method was proposed by Xu et al. [70] to increase the efficiency of building a mesoscale model of concrete and research the influence of ITZ on the diffusivity of concrete.

2.5. Combined Particle Method

In addition to the aggregate modeling techniques mentioned above, another method combines simple basic particles to construct complex composite particles. The combination sphere method, proposed by Favier et al. [71,72], is currently the most common method in the combined particle method. It combines a specific number of spherical particles in an overlapping arrangement to form a composite particle.

Some researchers have used combined spheres that are not permitted to overlap to combine irregular particles for modeling purposes [73]. This method bears some similarities to voxel-based methods. Compared to the combined particle method, in which basic particles are allowed to overlap, this method improved computational efficiency but reduced model accuracy.

Additionally, a spherosimplices method is also used in particle modeling. This method involves moving spheres along a linear triangle or another shaped skeleton to represent particles.

Indeed, the combined particle method is not limited to modeling with spheres and can incorporate other basic shapes, such as cylinders and rectangles, to construct complex particle shapes [74,75].

The combination particle method is extensively used in the modeling of concrete at the mesoscale [76,77]. However, each aggregate with a different shape needs to be remodeled once. When concrete has a large number of aggregates with different shapes, a large amount of computing resources will be used to model aggregates. The model accuracy and storage space of the combination particle method are influenced by the number of basic particles that compose the aggregate. For complex aggregates, more basic particles are needed to build an aggregate model. Higher numbers of basic particles enhance authenticity but also increase storage space.

2.6. Summary

When modeling aggregates, it is necessary to select an appropriate method based on the computational cost and the accuracy requirements of the modeling. Three aspects must be considered when choosing a modeling method, including model accuracy, storage space, and efficiency. It should be emphasized that accuracy refers to the degree of similarity between the model and aggregates when modeling complex-shaped aggregates with the otherwise same conditions. The efficiency refers to the computational resources consumed when modeling complex-shaped aggregates with the otherwise same conditions. Table 1 summarizes the advantages and disadvantages of various aggregate modeling methods from these four aspects.

Table 1. Comparisons between the different modeling approaches for aggregate modeling.

	Model Accuracy	Model Storage Space and Modeling Efficiency
Virtual Space Method	Influenced by the density of the grid division and accuracy is middle.	Large storage space and middle modeling efficiency.
Polygon and Polyhedron Method	Accuracy for polygon and polyhedron is high. Accuracy for others is low.	Large storage space and high modeling efficiency.
Continuous Function Method	Accuracy for spherical, ellipsoid, etc., is high. Accuracy for complex shapes is influenced by spherical harmonics calculate order. The accuracy is middle.	Small storage space and high modeling efficiency for spheres and ellipsoids, and lower modeling efficiency for complex shapes.
Discrete Function Method	Influenced by the density of the discrete points, and accuracy is middle.	Large storage space and low modeling efficiency. It is commonly used in modeling based on continuous function algorithms.
Combined Particle Method	Influenced by the number of basic particles and accuracy is low.	Middle storage space and low modeling efficiency.

3. Collision Detection Algorithm

After building the aggregate model, the second stage of building a mesoscale model of concrete is detecting the collision between aggregate models. There are certain theoretical foundations that should be introduced in order to better comprehend collision detection algorithms. The collision of aggregates is an inevitable occurrence when constructing a mesoscale model. The detection of such collisions constitutes the core content of building a mesoscale model of concrete. The theoretical foundations pertaining to the detection of such collisions will be summarized. Based on the theoretical foundations, the choice of the collision detection algorithm is a crucial step in building a mesoscale model of concrete. The choice of the collision detection algorithm depends on the storage format of the aggregate models. Although the storage format of the aggregate can be converted, the change process consumes a lot of computing time. In this way, this section introduces collision detection algorithms that correspond to the aggregate modeling methods. Contact detection can be

divided into a spatial sorting phase and a contact resolution phase. The spatial sorting phase avoids all-to-all aggregate collision detection by screening aggregates that may collide. The contact resolution phase detects the details of the contact between aggregates. There are five prevalent types of aggregate modeling methods and their corresponding collision detection algorithms in the contact resolution phase: the virtual space method with voxel-based detection algorithms; polygon polyhedron methods with separation axis common plane algorithms; continuous function methods with the geometric potential algorithm; discrete function methods with the simplified geometric potential algorithm; and combined particle methods with the combined particle collision detection method. In general, a collision detection algorithm is deemed superior if it has high detection efficiency and detection accuracy. In this section, the collision detection algorithm in the spatial sorting phase is sketched, and various methods of collision detection algorithms in the contact resolution phase and the theoretical foundations are summarized.

3.1. Spatial Sorting Phase

Spatial sorting algorithms try to lock aggregates that may collide to avoid the detailed collision detection of all aggregates. Through this phase, the efficiency of the collision detection is improved. Some spatial sorting algorithms, including the grid subdivision method, adaptive grid method, octree method, body-based cells, and spatial heapsort, have been proposed to improve computational efficiency [78]. Among them, the grid subdivision method and adaptive grid method are commonly used methods.

The grid subdivision method disperses the concrete model into cells uniformly. Every cell contains zero or more aggregates, and every cell is still associated with all the aggregates inside it. When searching for aggregates that may collide with aggregate A, only the aggregates in the cells near the associated cells of aggregate A need to be considered. This method needs to balance the size of the cell and the number of aggregates. When the aggregates are distributed in the concrete model evenly, the spatial sorting method will yield good results. If all the aggregates are clustered in one cell, this method will yield no advantage [67]. To overcome the spatial heterogeneity of the grid subdivision method, the adaptive grid method was proposed. In this method, the model is divided by a cutting plane, and there is approximately the same number of aggregates on either side of the cutting plane. However, when the aggregates are distributed in the model evenly, the grid subdivision method consumes additional computing resources to calculate the cutting plane [79].

3.2. Voxel-Based Detection Algorithms

The voxel-based detection algorithms for virtual space method collision detection are illustrated in Figure 6. The concrete model is discretized into voxels, with the occupied voxels being marked to denote the presence of aggregates. The algorithm iterates through all the voxels, and if a voxel is marked by multiple aggregates, it indicates a collision.

Virtual space methods offer a straightforward representation of particles with arbitrary shapes. The voxel-based detection algorithms are relatively straightforward and provide comprehensive information regarding aggregate collisions [80]. The accuracy and efficiency of voxel-based detection algorithms depend on the resolution of aggregate models. With the increase in resolution, the accuracy of collision detection will be improved but the efficiency will be reduced [41].

			b	b	b
			b	b	b
a	a	a	b	b	b
a	a	a			
a	a	a			

Figure 6. Two-dimensional illustration of a packing matrix containing two distinct particles. Each particle is described by a set of voxels identified by the id of the particle [41].

3.3. Common Plane Separation Axis Algorithms

The common plane separation axis algorithm is used to detect the collision of the aggregate model built by the polygon polyhedron method. In 1988, Cundall [81] introduced the common plane algorithm for collision detection between convex polyhedral aggregates. This algorithm identifies a common face that bisects the space between two convex polyhedral particles. If this common face intersects both aggregates, a collision is detected; otherwise, no collision is reported. The key aspect of this method lies in the identification of the common face, which involves determining an initial plane and performing multiple corrective iterations. Nezami et al. [82] proposed the shortest link method and a fast algorithm based on the original common face algorithm to expedite the common face identification process.

Another frequently used algorithm for collision detection between polygons or polyhedrons is the separation axis algorithm. For polygons, if a normal vector exists for one side such that the projections of the particles on this vector do not overlap, it can be concluded that the two polygons do not collide. Similarly, for a polyhedron, if a normal vector exists for one face or edge such that the projections of the particles on this vector do not overlap, it can be concluded that the two polyhedrons do not collide [83,84].

The common plane separation axis algorithms can detect collision between two different aggregate models accurately and efficiently. The subsequent operations, such as rotations and displacements, are uncomplicated, with only vertex coordinates requiring transformation during rotations and displacements. However, the information regarding aggregate collisions cannot be obtained from the common plane separation axis algorithms directly.

3.4. Geometric Potential Algorithm

The geometric potential algorithm has been widely used to detect the collisions of aggregates modeled by the continuous function method. This algorithm combines the surface functions of the aggregates to formulate a contact equation. By examining whether the collision equation possesses a solution, it is determined whether a collision has occurred

between the aggregates. This particular method is commonly employed when dealing with aggregates characterized by relatively simple surface functions, such as spheres.

Ng [85] and Ting [86] introduced the concept of the geometric potential as a means to detect collisions between aggregates. Figure 7 illustrates their approach, where a set of concentric ellipses is constructed both inside and outside the examined ellipse 1 and ellipse 2. Points lying on the same concentric ellipse exhibit identical geometric potential. Specifically, the geometric potential of points located within ellipse 1 and ellipse 2 is negative, whereas the geometric potential of points situated outside ellipse 1 and ellipse 2 is positive. Notably, there exists point P_1 on ellipse 1, which possesses the lowest geometric potential relative to P_2 . If the geometric potential of point P_1 to ellipse 2 is less than zero, it implies that P_1 lies within ellipsoid 2, representing that a collision has occurred between the two aggregates [87].

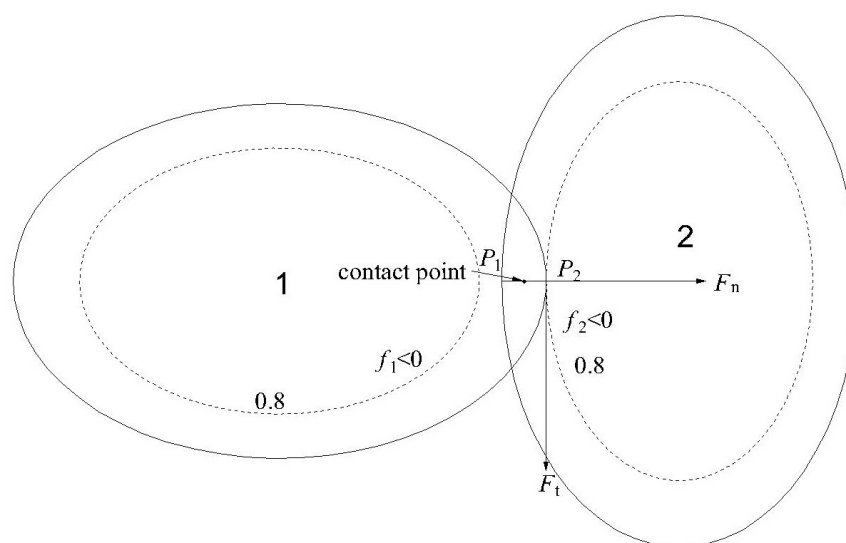


Figure 7. Definition of the overlap and contact normal of super-quadric particles based on the geometric potential concept [87].

To achieve collision detection that aligns more closely with the mechanical definition of collision, Lin and Ng [88] proposed the common normal vector method based on the geometric potential algorithm. This algorithm identifies collision points that are more consistent with the mechanical interpretation of collision, although it necessitates the increased computational time. Džiugys and Peters [80] further optimized the geometric potential algorithm by streamlining the calculation process for the point with the lowest geometric potential.

Qian [89] conducted collision detection based on contact equations for aggregate models of arbitrary shapes. Initially, spherical harmonic functions were utilized to model the aggregates and derive their respective surface functions. Subsequently, the surface functions were combined to establish contact equations between the aggregates. Finally, the Newton–Raphson iteration method was employed to solve the contact equations, enabling collision detection between particles with complex shapes based on these contact equations.

The geometric potential algorithm can detect collisions of aggregates accurately and obtain comprehensive information regarding aggregate collisions. However, multiple iterations, which lead to increased computational costs, are needed when using contact equations to detect collisions between complex particles.

3.5. Simplified Geometric Potential Algorithm

The discrete function method serves as an alternative to the continuous function method by replacing the particle's surface function with discrete points on the surface. In this method, the invasion of one particle by another is determined by comparing the

geometric potential of discrete points on the surface [90,91]. If the geometric potential of a discrete point on the surface of particle 1 to particle 2 is less than zero, it indicates that the discrete point on the surface of particle 1 has invaded particle 2. Therefore, in the discrete function method, the geometric potential method is simplified, eliminating the need to find the minimum geometric potential point. Instead, the discrete points on the particle surface are traversed to identify any points that have invaded other particles [58,87,92].

By a simplified geometric potential algorithm, comprehensive aggregate collision information can be obtained. The accuracy and efficiency of the simplified geometric potential algorithm depend on the number of discrete points. With the increase in the number of discrete points, the accuracy of the collision detection is improved, but the efficiency is reduced.

3.6. Combined Particle Collision Detection Method

This method detects collisions between composite particles by examining collisions between basic particles. However, due to the disparity between the combined sphere model and the original particle, the smooth surface of the original particle becomes uneven, resulting in a single collision between composite particles being recognized as multiple collisions. This discrepancy is illustrated in Figure 8, where a single contact point between a sphere and a plane becomes three contact points in the spherical particles produced by the composite particles. Consequently, when calculating the contact force between particles, a significant error arises [93].

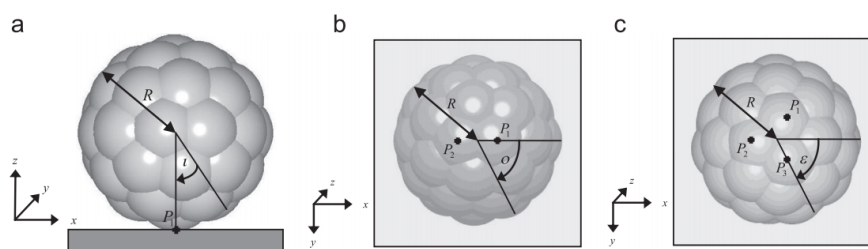


Figure 8. Definition of the overlap and normal contact of super-quadric particles based on the geometric potential concept [87].

Kruggel-Emden et al. [94] utilized the combination particle method to model spherical particles and conducted numerical simulations of impact tests involving these particles striking a flat wall. The results revealed that using the combination sphere method to model composite particles led to significant errors. Kodam et al. [95] made revisions to the force model generated by particle contact and attempted to address this issue, but a complete resolution was not achieved. Additionally, calculating the mass and moment of inertia of composite particles becomes complex when allowing spherical particles to overlap with one another. Despite these challenges, the combination sphere method remains a relatively accurate particle modeling technique. Markauskas et al. [96] employed the combination sphere method to model ellipsoids and compared the angle of repose of smooth ellipsoids with that of the combination sphere models. The results demonstrated that as the number of component spheres increased, the angle of repose of the combination sphere model gradually converged with that of the smooth ellipsoids.

Galindo-Torres and Pedroso [97] introduced a collision detection algorithm to address the issue of collisions between particles modeled using the spherosimplices method. The algorithm first determines the shortest distance between the two particle skeletons and then compares this distance with the sum of the radii of the two moved spheres to determine whether a collision has occurred between the particles.

However, when using multiple basic shapes to model particles, collisions between different basic particles need to be considered. This problem makes the process of collision detection become more intricate.

Collision detection efficiency will decrease with the increase in the number of basic particles. Models created with the combination particle method are prone to recognizing a single collision point as multiple collision points during collision detection. Furthermore, obtaining collision detection information between aggregates requires solving collision equations between basic particles, which is relatively complex compared to discrete function methods and voxel-based methods.

3.7. The Definition of Collision

The definition of collision has a significant impact on the movement of aggregates. As such, it is imperative to elucidate how collisions are defined and which key information pertaining to collisions should be obtained. As depicted in Figure 9, for 2D circular aggregates, R_1 and R_2 represent the radii of the circles, while C_1 and C_2 represent their respective centers. B_1 and B_2 denote the intersections of C_1C_2 with the circles. The overlap length δ between the two circles can be defined as B_1B_2 . The contact point P is defined as the midpoint of B_1B_2 . The contact normal is defined by the vector C_1C_2 , while the tangential direction of the contact is given by the direction perpendicular to C_1C_2 . For non-spherical aggregates, there is no consensus on the definition of the collision information. In summary, it is necessary to obtain information pertaining to the overlap length, contact point, contact normal, and tangential direction of the collision [98].

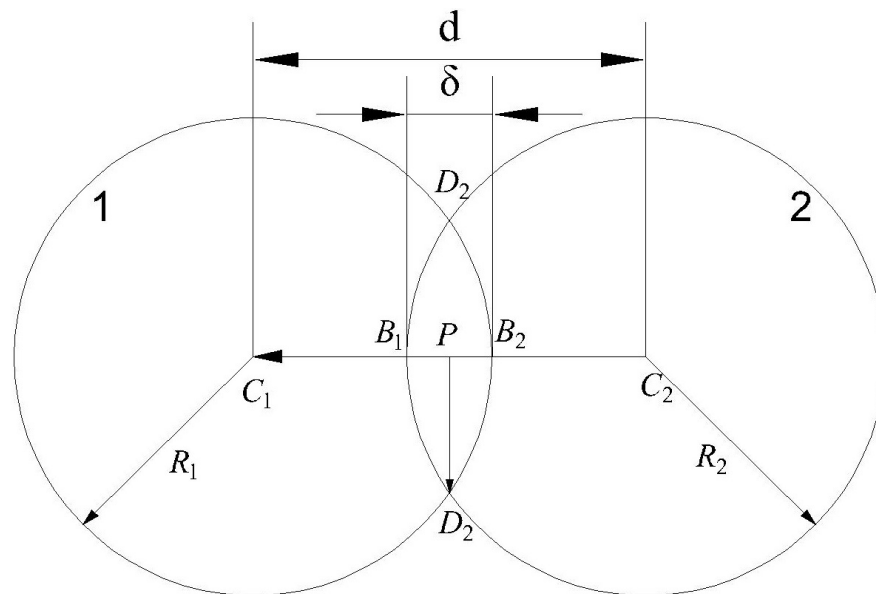


Figure 9. Definition of the contact point, contact normal and tangential, and contact overlap for two colliding identical spheres [98].

3.8. Summary

There are several factors that must be considered when evaluating a collision detection algorithm. These include the collision detection accuracy and efficiency of collision detection. Table 2 summarizes the characteristics of various collision detection algorithms as follows. It should be highlighted that accuracy refers to whether the algorithm can accurately determine whether there is a collision between aggregates and accurately calculate the basic information of the collision. The efficiency refers to the computational resources consumed when detecting aggregate collisions.

Table 2. Comparisons of the different modeling approaches for collision detection.

	Correspond Aggregate Modeling Method	Collision Detection Accuracy	Efficiency of Collision Detection
Voxel-based collision detection algorithm	Virtual Space Method	Related to the density of the virtual space grid partitioning and accuracy is middle.	Related to the density of the virtual space grid partitioning.
Separation axis common plane algorithms	Polygon and Polyhedron Method	High	High
Geometric Potential Algorithm	Continuous Function Method	High	Low
Simplified Geometric Potential Algorithm	Discrete Function Method	Related to the density of the discrete points and accuracy is middle.	Related to the density of the discrete points.
Combined Particle Collision Detection Method	Combined Particle Method	Related to the density of the number of basic particles and accuracy is low.	Related to the number of basic particles.

4. The Aggregate Packing Algorithm

The aggregate packing algorithm is a fundamental approach for incorporating aggregates into concrete models. The commonly used algorithms can be categorized into the following five types: the random sequential packing algorithm, the sequential deposition algorithm, the collective rearrangement algorithm, the Voronoi tessellation algorithm, and the CT image algorithm. An effective aggregate packing algorithm plays a crucial role in creating a precise concrete representation while achieving a higher volume fraction in the model.

4.1. The Random Sequential Packing Algorithm

The random sequential packing algorithm, which is also known as the Monte Carlo algorithm, stands as one of the most widely employed methods for aggregate packing [6,52]. Within this algorithm, aggregates are put into the concrete one by one in order from largest to smallest. Each aggregate is assigned a random coordinate and an initial orientation when it is put into the concrete. Subsequently, it is examined whether any collisions occur between the aggregate and the aggregates already placed. A new coordinate is randomly generated until no collisions are detected.

The random sequential packing algorithm operates on a simple principle and results in a concrete model with excellent randomness. However, the volume fraction of the concrete model tends to be lower. Cooper [99] utilized the random sequential packing algorithm to construct a sphere pack model, demonstrating that the packing-limit volume fraction of single-size spheres reaches approximately 0.385 [99]. On this basis, aggregate gradation is also considered in the concrete mesoscale model. Xu and Chen [52] use random sequential packing algorithm to build a cement model and assess the effect of particle size distribution on the random packing of the dodecahedral particles. Huang et al. [6] used Monte Carlo simulations of 2D and 3D mesoscale concrete to research the dynamic damage and fracture behavior of concrete. It becomes challenging to incorporate the last few aggregates into the concrete model, as the trial aggregate possesses a high probability of colliding with existing aggregates.

4.2. The Sequential Deposition Algorithm

In contrast to the random sequential packing algorithm, Visscher and Bolsterli [100] introduced the sequential deposition algorithm, which offers a partial simulation of the aggregate falling process. In this algorithm, aggregates are dropped sequentially from a random point located at the top of the concrete model. Upon collision with other aggregates, the new dropped aggregate initiates a rolling motion. The rolling ceases once the aggregate reaches a stable position. For monosized spheres, stability is achieved when the sphere contacts three other spheres or the underside of the concrete model. The sequential

deposition algorithm allows for the simulation of aggregate packing processes and yields higher volume fractions compared to the random sequential packing algorithm. In this way, the sequential deposition algorithm is widely used in the modeling of particle accumulation models [101,102].

However, the arrangement of aggregates may still lack compactness. To address this concern, Visscher and Bolsterli [100] proposed a method to enhance the volume fraction. This method involves conducting multiple attempts at depositing aggregates and identifying the lowest (minimum energy) positions to simulate the shaking of the model. In the case of monosized spheres, the volume fraction of the concrete model can reach up to 58%. Shashidhar and Gopalakrishnan [101] studied the aggregate structure in hot-mix asphalt under the consideration of aggregate gradation.

4.3. The Collective Rearrangement Algorithm

The collective rearrangement algorithm represents a category of packing algorithms commonly used in conjunction with other aggregate packing methods [103–106]. Typically, an initial concrete model is constructed using the sequential deposition algorithm or the random sequential packing algorithm. During the initial stage, numerous particles are placed in a confined space, allowing for overlapping. Subsequently, various algorithms employ different techniques to eliminate the overlap [107].

One such algorithm is the force-biased algorithm proposed by Jodrey and Tory [107]. It involves moving all aggregates and reducing their sizes until the overlap is eliminated. Jodrey and Tory [107] utilized this algorithm to construct a packing model, achieving a volume fraction of 64.2–64.9% when the particles were equal-sized spheres. Another collective rearrangement algorithm was introduced by Lubachevsky and Stillinger [108]. Their method begins with a random distribution of points, which then undergo random movements and expansion during the simulation. Donev et al. [109] employed Lubachevsky and Stillinger's approach to creating an ellipsoid packing model with a volume fraction of 74%. Both the force-biased algorithm and Lubachevsky and Stillinger's method involve modifying the particle sizes during the packing process.

In contrast, He et al. [110] proposed a novel method that eliminates overlap without altering the particle sizes. Their approach incorporates particle movement considering gradation. Similarly, Williams and Philipse [111] introduced the mechanical contraction algorithm, which also accounts for gradation in the particle packing model. This algorithm begins by constructing a dilute particle packing model using the Monte Carlo method. This initial model is then compressed to achieve a higher volume fraction by reducing the model's volume and scaling all particle coordinates accordingly. Trofimov et al. [112] used an algorithm based on the modified collective rearrangement method to build a fiber concrete model, and the elastic properties of fiber concrete were researched.

Although the collective rearrangement algorithm generally results in higher volume fractions compared to the sequential deposition algorithm or the random sequential packing algorithm, it does have certain drawbacks. The iterative nature of particle coordinate calculations in the packing process can lead to longer computation times.

4.4. The Voronoi Tessellation Algorithm

The Voronoi tessellation method was initially used for modeling crystalline materials and has since been applied to granular material modeling. The first step of this method involves generating Voronoi cells. These cells fill the model space. Subsequently, there are two approaches to generating the concrete model. In the first approach, different attributes, such as aggregates or cement, are assigned to distinct Voronoi cells. In the second approach, the Voronoi cells are contracted, with the cells themselves representing aggregates and the spaces between them representing cement. The Voronoi tessellation method allows for the straightforward generation of mesoscale models of concrete with high-volume fractions [113].

4.5. The CT Image Algorithm

The CT image method is becoming increasingly popular for constructing mesoscale models of concrete. Advanced facilities, such as X-ray computed tomography (XCT) scanners, are now commonly used to acquire digital images of real concrete samples at the mesoscale level [9,114,115]. These XCT images can be directly converted into mesoscale models of concrete. One of the significant advantages of this method is that it provides direct access to the real size, shape, and distribution of aggregates and cement, eliminating the need for assumptions required in other aggregate modeling methods.

However, it is important to note that the CT image method can be costly and time consuming. Conducting XCT tests and processing the acquired images can be resource intensive. Additionally, when a significant number of samples are needed to perform meaningful statistical analyses, the costs associated with XCT can become more challenging to manage.

4.6. Summary

When conducting particle-packing simulations, different algorithms are adopted depending on the focus of the study. There are certain considerations that must be taken into account when numerically simulating aggregate packing. Questions that need to be addressed include the efficiency of the packing algorithm, the cost associated with using a specific packing method, whether the packing algorithm can simulate the packing process of aggregates, the maximum achievable volume fraction of aggregates in the packing model, and whether the packing algorithm can handle aggregates with arbitrary shapes and size distributions. This paper summarizes the characteristics of various particle-packing algorithms in Table 3.

Table 3. Comparisons between the different modeling approaches for aggregate packing.

	Packing Efficiency	Algorithm Cost	Packing Process	Volume Fraction *	Aggregates Shape	Aggregate Gradations
Random Sequential Packing Algorithm	Low volume fraction: High High volume fraction: Low	Low	No	0.385 [99]	Arbitrarily	Yes
Sequential Deposition Algorithm	Middle	Low	Yes	0.58 [100]	Arbitrarily	Yes
Collective Rearrangement Algorithm	Low	Low	No	0.64 [107]	Arbitrarily	Yes
Voronoi Tessellation algorithm	High	Low	No	---	Arbitrarily	Yes
CT Image Algorithm	High	High	No	---	---	No

* The volume fraction in the table represents the maximum achievable volume fraction when using a single-sized spherical particle for packing using the respective algorithm.

5. Conclusions

This paper provides an overview of the current state of mesoscale modeling methods for concrete based on existing literature. The theoretical foundations of concrete mesoscale modeling are initially discussed, followed by an exploration of various methods for the three essential steps of concrete modeling: aggregate modeling, collision detection algorithms, and particle-packing algorithms. Based on this review, the following conclusions can be drawn.

1. The choice of the aggregate modeling method depends on the requirement of the model accuracy.
2. The choice of the collision detection algorithm is often influenced by the selected aggregate modeling method, although this relationship is not absolute.
3. To build models that are reasonable and effective, it is crucial to select mutually adaptive methods for the three modeling steps based on specific requirements and available resources.

Benefiting from the collective effort of numerous scholars, concrete mesoscale modeling has made significant progress in recent years. However, there are still some limitations for concrete mesoscale modeling. In our view, the concrete mesoscale modeling can be improved from the three aspects of accuracy, packing fraction, and efficiency as follows.

1. Accuracy. Although the concrete mesoscale modeling method based on the real aggregate shape has been developed, the most commonly used concrete mesoscale modeling method is still based on regular aggregate shapes. There are a few promising methods that have been proposed. The first one is directly obtaining the mesoscale model of concrete by X-ray CT [114,116]. The second one is obtaining the shape of real aggregates by X-ray CT or laser scanning to build the library of aggregate. The aggregate model in the library will be packed to model concrete at the mesoscale [89], but both of these methods are needed to solve the high cost which is produced in the scan.
2. Packing fraction. The random sequential packing algorithm is the most commonly used algorithm. However, the packing fraction of concrete modeled by the random sequential packing algorithm is limited. In order to obtain the concrete model with a higher packing fraction, some more advanced algorithms have been used. Based on the concrete model built by other packing algorithms, a dynamic physics engine can be used to simulate compaction and vibration and improve the packing fraction [117].
3. Efficiency. As the packing fraction increases, the computational efficiency will inevitably decrease. However, the efficiency must be controlled within an acceptable range. For this goal, researchers have tried to simplify the collision detection algorithm and propose a more efficient packing algorithm [9]. The parallel computing and GPU-based acceleration methods are also used to improve computational efficiency [118].

Author Contributions: Conceptualization, Z.P. and J.Z.; methodology, J.Z.; software, J.Z.; validation, R.M., Z.P. and H.Z.; formal analysis, J.Z.; investigation, J.Z.; resources, J.Z.; data curation, H.Z.; writing—original draft preparation, J.Z.; writing—review and editing, Z.P.; visualization, J.Z.; supervision, R.M.; project administration, R.M.; funding acquisition, R.M. All authors have read and agreed to the published version of the manuscript.

Funding: This research project was financially supported by the National Natural Science Foundation of China under the Grant No. 52238005 and the National Key R & D Program of China (Grant No. 2021YFF0501003).

Data Availability Statement: The data presented in this study are available in the respective references.

Conflicts of Interest: The authors declare no conflict of interest.

References

1. Nguyen, V.P.; Stroeven, M.; Sluys, L.J. Multiscale failure modeling of concrete: Micromechanical modeling, discontinuous homogenization and parallel computations. *Comput. Methods Appl. Mech. Eng.* **2012**, *201*, 139–156. [\[CrossRef\]](#)
2. Wriggers, P.; Moftah, S. Mesoscale models for concrete: Homogenisation and damage behaviour. *Finite Elem. Anal. Des.* **2006**, *42*, 623–636. [\[CrossRef\]](#)
3. Chen, H.; Sun, W.; Stroeven, P. Interfacial transition zone between aggregate and paste in cementitious composites (II): Mechanism of formation and degradation of interfacial transition zone microstructure, and its influence factors. *Kuei Suan Jen Hsueh Pao/J. Chin. Ceram. Soc.* **2004**, *32*, 70–79.
4. Zhou, X.; Hao, H. Mesoscale modelling of concrete tensile failure mechanism at high strain rates. *Comput. Struct.* **2008**, *86*, 2013–2026. [\[CrossRef\]](#)
5. Pedersen, R.; Simone, A.; Sluys, L. Mesoscopic modeling and simulation of the dynamic tensile behavior of concrete. *Cem. Concr. Res.* **2013**, *50*, 74–87. [\[CrossRef\]](#)

6. Huang, Y.; Yang, Z.; Chen, X.; Liu, G. Monte Carlo simulations of meso-scale dynamic compressive behavior of concrete based on X-ray computed tomography images. *Int. J. Impact Eng.* **2016**, *97*, 102–115. [[CrossRef](#)]
7. Zhou, Y.; Jin, H.; Wang, B. Modeling and mechanical influence of meso-scale concrete considering actual aggregate shapes. *Constr. Build. Mater.* **2019**, *228*, 116785. [[CrossRef](#)]
8. Li, C.Z.; Song, X.B. Mesoscale modeling of chloride transport in unsaturated concrete based on Voronoi tessellation. *Cem. Concr. Res.* **2022**, *161*, 106932. [[CrossRef](#)]
9. Huang, L.; Tang, L.; Löfgren, I.; Olsson, N.; Yang, Z.; Li, Y. Moisture and ion transport properties in blended pastes and their relation to the refined pore structure. *Cem. Concr. Res.* **2022**, *161*, 106949. [[CrossRef](#)]
10. Yao, L.; Ren, L.; Gong, G.; Zhang, J. Simulation of chloride diffusion in concrete based on a new mesoscopic numerical method. *Adv. Civ. Eng.* **2020**, 2020. [[CrossRef](#)]
11. Wittmann, F. Structure of concrete with respect to crack formation. *Fract. Mech. Concr.* **1983**, *43*, 6.
12. Bažant, Z.P.; Tabbara, M.R.; Kazemi, M.T.; Pijaudier-Cabot, G. Random particle model for fracture of aggregate or fiber composites. *J. Eng. Mech.* **1990**, *116*, 1686–1705. [[CrossRef](#)]
13. Zubelewicz, A.; Bažant, Z.P. Interface element modeling of fracture in aggregate composites. *J. Eng. Mech.* **1987**, *113*, 1619–1630. [[CrossRef](#)]
14. Vonk, R. Softening of Concrete Loaded in Compression. Ph.D. Thesis, Built Environment, Technische Universiteit Eindhoven, Eindhoven, The Netherlands, 1992.
15. Cusatis, G.; Bažant, Z.P.; Cedolin, L. Confinement-shear lattice model for concrete damage in tension and compression: I. Theory. *J. Eng. Mech.* **2003**, *129*, 1439–1448. [[CrossRef](#)]
16. Cusatis, G.; Mencarelli, A.; Pelessone, D.; Baylot, J. Lattice discrete particle model (LDPM) for failure behavior of concrete. II: Calibration and validation. *Cem. Concr. Compos.* **2011**, *33*, 891–905. [[CrossRef](#)]
17. Schlangen, E.; Garboczi, E.J. Fracture simulations of concrete using lattice models: Computational aspects. *Eng. Fract. Mech.* **1997**, *57*, 319–332. [[CrossRef](#)]
18. Lilliu, G.; van Mier, J.G. 3D lattice type fracture model for concrete. *Eng. Fract. Mech.* **2003**, *70*, 927–941. [[CrossRef](#)]
19. Caballero, A.; Carol, I.; López, C. A meso-level approach to the 3D numerical analysis of cracking and fracture of concrete materials. *Fatigue Fract. Eng. Mater. Struct.* **2006**, *29*, 979–991. [[CrossRef](#)]
20. Nagai, K.; Sato, Y.; Ueda, T. Mesoscopic simulation of failure of mortar and concrete by 3D RBSM. *J. Adv. Concr. Technol.* **2005**, *3*, 385–402. [[CrossRef](#)]
21. Avadh, K.; Jiradilok, P.; Bolander, J.E.; Nagai, K. 3D mesoscale simulation of the influence of corrosion on loss of tension stiffening in reinforced concrete. *Constr. Build. Mater.* **2022**, *339*, 127684. [[CrossRef](#)]
22. Hentz, S.; Daudeville, L.; Donzé, F.V. Identification and validation of a discrete element model for concrete. *J. Eng. Mech.* **2004**, *130*, 709–719. [[CrossRef](#)]
23. Azevedo, N.M.; Lemos, J. Aggregate shape influence on the fracture behaviour of concrete. *Struct. Eng. Mech. Int. J.* **2006**, *24*, 411–427. [[CrossRef](#)]
24. Nitka, M.; Tejchman, J. Modelling of concrete behaviour in uniaxial compression and tension with DEM. *Granul. Matter* **2015**, *17*, 145–164. [[CrossRef](#)]
25. Zhou, W.; Zhao, C.; Liu, X.; Chang, X.; Feng, C. Mesoscopic simulation of thermo-mechanical behaviors in concrete under frost action. *Constr. Build. Mater.* **2017**, *157*, 117–131. [[CrossRef](#)]
26. Tal, D.; Fish, J. Stochastic multiscale modeling and simulation framework for concrete. *Cem. Concr. Compos.* **2018**, *90*, 61–81. [[CrossRef](#)]
27. Alnaggar, M.; Cusatis, G.; Di Luzio, G. Lattice discrete particle modeling (LDPM) of alkali silica reaction (ASR) deterioration of concrete structures. *Cem. Concr. Compos.* **2013**, *41*, 45–59. [[CrossRef](#)]
28. Serra, C.; Azevedo, N.M.; Lopes Batista, A.; Schlar, N. Discrete element method for modeling the long-term aging viscoelastic behavior of concrete considering its mesostructure. *J. Eng. Mech.* **2018**, *144*, 04018021. [[CrossRef](#)]
29. Wang, W.; Wang, J.; Wang, J.; He, J.; Pan, J. Mesoscale modeling study on mechanical deterioration of alkali–aggregate reaction-affected concrete. *Materials* **2022**, *15*, 3861. [[CrossRef](#)]
30. Reza khani, R.; Gallyamov, E.; Molinari, J.F. Meso-scale finite element modeling of Alkali-Silica-Reaction. *Constr. Build. Mater.* **2021**, *278*, 122244. [[CrossRef](#)]
31. Zhao, C.; Zhou, W.; Chen, X.; Wu, Q.; Ma, G.; Wang, Q. Mesoscopic analysis of heat and moisture coupled transfer in concrete considering phase change under frost action. *J. Build. Eng.* **2022**, *57*, 104888. [[CrossRef](#)]
32. Jin, L.; Yu, W.; Du, X.; Yang, W. Mesoscopic numerical simulation of dynamic size effect on the splitting-tensile strength of concrete. *Eng. Fract. Mech.* **2019**, *209*, 317–332. [[CrossRef](#)]
33. Vegt, I.; Breugel, V.; Weerheijm, J. Failure mechanisms of concrete under impact loading. *Fract. Mech. Concr. Concr. Struct. FraMCoS-6* **2007**, *1*, 579–587.
34. Bicanic, N.; Borst, R.; Mang, H.; Meschke, G. *Computational Modelling of Concrete Structures*; CRC Press: Boca Raton, FL, USA, 2010.
35. Ma, H.; Xu, W.; Li, Y. Random aggregate model for mesoscopic structures and mechanical analysis of fully-graded concrete. *Comput. Struct.* **2016**, *177*, 103–113. [[CrossRef](#)]

36. Comby-Peyrot, I.; Bernard, F.; Bouchard, P.O.; Bay, F.; Garcia-Diaz, E. Development and validation of a 3D computational tool to describe concrete behaviour at mesoscale. Application to the alkali-silica reaction. *Comput. Mater. Sci.* **2009**, *46*, 1163–1177. [[CrossRef](#)]
37. Pan, Z.; Chen, A.; Ruan, X. Spatial variability of chloride and its influence on thickness of concrete cover: A two-dimensional mesoscopic numerical research. *Eng. Struct.* **2015**, *95*, 154–169. [[CrossRef](#)]
38. Li, B.; Mao, J.; Nawa, T.; Liu, Z. Mesoscopic chloride ion diffusion model of marine concrete subjected to freeze-thaw cycles. *Constr. Build. Mater.* **2016**, *125*, 337–351. [[CrossRef](#)]
39. Zhao, S.; Zhang, N.; Zhou, X.; Zhang, L. Particle shape effects on fabric of granular random packing. *Powder Technol.* **2017**, *310*, 175–186. [[CrossRef](#)]
40. Jia, X.; Williams, R.A. A packing algorithm for particles of arbitrary shapes. *Powder Technol.* **2001**, *120*, 175–186. [[CrossRef](#)]
41. Byholm, T.; Toivakka, M.; Westerholm, J. Effective packing of 3-dimensional voxel-based arbitrarily shaped particles. *Powder Technol.* **2009**, *196*, 139–146. [[CrossRef](#)]
42. Abyaneh, S.D.; Wong, H.; Buenfeld, N. Modelling the diffusivity of mortar and concrete using a three-dimensional mesostructure with several aggregate shapes. *Comput. Mater. Sci.* **2013**, *78*, 63–73. [[CrossRef](#)]
43. Liu, C.; Liu, G.; Liu, Z.; Yang, L.; Zhang, M.; Zhang, Y. Numerical simulation of the effect of cement particle shapes on capillary pore structures in hardened cement pastes. *Constr. Build. Mater.* **2018**, *173*, 615–628. [[CrossRef](#)]
44. Abyaneh, S.D.; Wong, H.; Buenfeld, N. Computational investigation of capillary absorption in concrete using a three-dimensional mesoscale approach. *Comput. Mater. Sci.* **2014**, *87*, 54–64. [[CrossRef](#)]
45. Wang, M.; Al-Tabbaa, A.; Wang, W. Improving discrete particle packing models for the microstructural formation simulation of Portland cement. *Constr. Build. Mater.* **2019**, *229*, 116841. [[CrossRef](#)]
46. Jia, X.; Garboczi, E.J. Advances in shape measurement in the digital world. *Particuology* **2016**, *26*, 19–31. [[CrossRef](#)]
47. De Korte, A.; Brouwers, H. Random packing of digitized particles. *Powder Technol.* **2013**, *233*, 319–324. [[CrossRef](#)]
48. Ghaboussi, J.; Barbosa, R. Three-dimensional discrete element method for granular materials. *Int. J. Numer. Anal. Methods Geomech.* **1990**, *14*, 451–472. [[CrossRef](#)]
49. Kruggel-Emden, H.; Oschmann, T. Numerical study of rope formation and dispersion of non-spherical particles during pneumatic conveying in a pipe bend. *Powder Technol.* **2014**, *268*, 219–236. [[CrossRef](#)]
50. Zhao, S.; Zhou, X.; Liu, W. Discrete element simulations of direct shear tests with particle angularity effect. *Granul. Matter* **2015**, *17*, 793–806. [[CrossRef](#)]
51. Höhner, D.; Wirtz, S.; Scherer, V. Experimental and numerical investigation on the influence of particle shape and shape approximation on hopper discharge using the discrete element method. *Powder Technol.* **2013**, *235*, 614–627. [[CrossRef](#)]
52. Xu, W.; Chen, H. Numerical investigation of effect of particle shape and particle size distribution on fresh cement paste microstructure via random sequential packing of dodecahedral cement particles. *Comput. Struct.* **2013**, *114*, 35–45. [[CrossRef](#)]
53. Li, X.; Li, H.; Zhao, J. Transgranular fracturing of crystalline rocks and its influence on rock strengths: Insights from a grain-scale continuum–discontinuum approach. *Comput. Methods Appl. Mech. Eng.* **2021**, *373*, 113462. [[CrossRef](#)]
54. Fang, X.; Pan, Z.; Chen, A. Analytical models to estimate efficiency of capsule-based self-healing cementitious materials considering effect of capsule shell thickness. *Constr. Build. Mater.* **2021**, *274*, 121999. [[CrossRef](#)]
55. Pan, Z.; Ruan, X.; Chen, A. Chloride diffusivity of concrete: Probabilistic characteristics at meso-scale. *Comput. Concr.* **2014**, *13*, 187–207. [[CrossRef](#)]
56. Wu, B.; Yang, Y.; Zhang, L.; Wang, Y.; Li, H. Meso-scale numerical study on the non-uniform corrosion-induced cracking of confined concrete. *Constr. Build. Mater.* **2020**, *260*, 120463. [[CrossRef](#)]
57. Jin, L.; Hao, H.; Zhang, R.; Du, X. Determination of the effect of elevated temperatures on dynamic compressive properties of heterogeneous concrete: A meso-scale numerical study. *Constr. Build. Mater.* **2018**, *188*, 685–694. [[CrossRef](#)]
58. Hogue, C. Shape representation and contact detection for discrete element simulations of arbitrary geometries. *Eng. Comput.* **1998**, *15*, 374–390. [[CrossRef](#)]
59. Bowman, E.T.; Soga, K.; Drummond, W. Particle shape characterisation using Fourier descriptor analysis. *Geotechnique* **2001**, *51*, 545–554. [[CrossRef](#)]
60. Kiryati, N.; Maydan, D. Calculating geometric properties from fourier representation. *Pattern Recognit.* **1989**, *22*, 469–475. [[CrossRef](#)]
61. Wang, H.; Chen, Z.; Zhang, J.; Zheng, J.; Sun, X.; Li, J. Numerical scheme for predicting chloride diffusivity of concrete. *J. Mater. Civ. Eng.* **2021**, *33*, 04021237. [[CrossRef](#)]
62. Wei, D.; Hurley, R.C.; Poh, L.H.; Dias-da-Costa, D.; Gan, Y. The role of particle morphology on concrete fracture behaviour: A meso-scale modelling approach. *Cem. Concr. Res.* **2020**, *134*, 106096. [[CrossRef](#)]
63. Garboczi, E.J. Three-dimensional mathematical analysis of particle shape using X-ray tomography and spherical harmonics: Application to aggregates used in concrete. *Cem. Concr. Res.* **2002**, *32*, 1621–1638. [[CrossRef](#)]
64. Garboczi, E.J.; Bullard, J.W. 3D analytical mathematical models of random star-shape particles via a combination of X-ray computed microtomography and spherical harmonic analysis. *Adv. Powder Technol.* **2017**, *28*, 325–339. [[CrossRef](#)]
65. Bullard, J.W.; Garboczi, E.J. Defining shape measures for 3D star-shaped particles: Sphericity, roundness, and dimensions. *Powder Technol.* **2013**, *249*, 241–252. [[CrossRef](#)]
66. Cundall, P.A.; Strack, O.D.L. A discrete numerical model for granular assemblies. *Géotechnique* **1979**, *29*, 47–65. [[CrossRef](#)]

67. Williams, J.; O'Connor, R. A linear complexity intersection algorithm for discrete element simulation of arbitrary geometries. *Eng. Comput.* **1995**, *12*, 185–201. [[CrossRef](#)]
68. Liu, Y.; Gong, F.; You, Z.; Wang, H. Aggregate morphological characterization with 3D optical scanner versus X-ray computed tomography. *J. Mater. Civ. Eng.* **2018**, *30*, 04017248. [[CrossRef](#)]
69. Capozza, R.; Hanley, K. A hierarchical, spherical harmonic-based approach to simulate abradable, irregularly shaped particles in DEM. *Powder Technol.* **2021**, *378*, 528–537. [[CrossRef](#)]
70. Xu, W.; Jia, M.; Guo, W.; Wang, W.; Zhang, B.; Liu, Z.; Jiang, J. GPU-based discrete element model of realistic non-convex aggregates: Mesoscopic insights into ITZ volume fraction and diffusivity of concrete. *Cem. Concr. Res.* **2023**, *164*, 107048. [[CrossRef](#)]
71. Favier, J.F.; Abbaspour-Fard, M.H.; Kremmer, M. Modeling nonspherical particles using multisphere discrete elements. *J. Eng. Mech.* **2001**, *127*, 971–977. [[CrossRef](#)]
72. Favier, J.F.; Abbaspour-Fard, M.H.; Kremmer, M.; Raji, A.O. Shape representation of axi-symmetrical, non-spherical particles in discrete element simulation using multi-element model particles. *Eng. Comput.* **1999**, *16*, 467–480. [[CrossRef](#)]
73. Bertei, A.; Chueh, C.C.; Pharoah, J.; Nicoletta, C. Modified collective rearrangement sphere-assembly algorithm for random packings of nonspherical particles: Towards engineering applications. *Powder Technol.* **2014**, *253*, 311–324. [[CrossRef](#)]
74. Kodam, M.; Curtis, J.; Hancock, B.; Wassgren, C. Discrete element method modeling of bi-convex pharmaceutical tablets: Contact detection algorithms and validation. *Chem. Eng. Sci.* **2012**, *69*, 587–601. [[CrossRef](#)]
75. Song, Y.; Turton, R.; Kayihan, F. Contact detection algorithms for DEM simulations of tablet-shaped particles. *Powder Technol.* **2006**, *161*, 32–40. [[CrossRef](#)]
76. Chung, Y.C.; Ooi, J.Y. A study of influence of gravity on bulk behaviour of particulate solid. *Particuology* **2008**, *6*, 467–474. [[CrossRef](#)]
77. Yang, X.; You, Z.; Jin, C.; Wang, H. Aggregate representation for mesostructure of stone based materials using a sphere growth model based on realistic aggregate shapes. *Mater. Struct.* **2016**, *49*, 2493–2508. [[CrossRef](#)]
78. Huang, P.; Ding, Y.; Miao, Q.; Sang, G.; Jia, M. An improved contact detection algorithm for bonded particles based on multi-level grid and bounding box in DEM simulation. *Powder Technol.* **2020**, *374*, 577–596. [[CrossRef](#)]
79. Löhner, R. Automatic unstructured grid generators. *Finite Elem. Anal. Des.* **1997**, *25*, 111–134. [[CrossRef](#)]
80. Džiugys, A.; Peters, B. An approach to simulate the motion of spherical and non-spherical fuel particles in combustion chambers. *Granul. Matter* **2001**, *3*, 231–266. [[CrossRef](#)]
81. Cundall, P. Formulation of a three-dimensional distinct element model—Part I. A scheme to detect and represent contacts in a system composed of many polyhedral blocks. *Int. J. Rock Mech. Min. Sci. Geomech. Abstr.* **1988**, *25*, 107–116. [[CrossRef](#)]
82. Nezami, E.G.; Hashash, Y.M.; Zhao, D.; Ghaboussi, J. Shortest link method for contact detection in discrete element method. *Int. J. Numer. Anal. Methods Geomech.* **2006**, *30*, 783–801. [[CrossRef](#)]
83. Torquato, S.; Jiao, Y. Dense packings of polyhedra: Platonic and Archimedean solids. *Phys. Rev. E* **2009**, *80*, 041104. [[CrossRef](#)]
84. Xu, W.; Chen, H.; Liu, L. Evaluation of mesostructure of particulate composites by quantitative stereology and random sequential packing model of mono-/polydisperse convex polyhedral particles. *Ind. Eng. Chem. Res.* **2013**, *52*, 6678–6693. [[CrossRef](#)]
85. Ng, T.T. Numerical simulations of granular soil using elliptical particles. *Comput. Geotech.* **1994**, *16*, 153–169. [[CrossRef](#)]
86. Ting, J.M. A robust algorithm for ellipse-based discrete element modelling of granular materials. *Comput. Geotech.* **1992**, *13*, 175–186. [[CrossRef](#)]
87. Lu, G.; Third, J.; Müller, C. Critical assessment of two approaches for evaluating contacts between super-quadric shaped particles in DEM simulations. *Chem. Eng. Sci.* **2012**, *78*, 226–235. [[CrossRef](#)]
88. Lin, X.; Ng, T.T. Contact detection algorithms for three-dimensional ellipsoids in discrete element modelling. *Int. J. Numer. Anal. Methods Geomech.* **1995**, *19*, 653–659. [[CrossRef](#)]
89. Qian, Z. Multiscale Modeling of Fracture Processes in Cementitious Materials. Ph.D. Thesis, Technische Universiteit Delft, Delft, The Netherlands, 2012.
90. Lu, G.; Third, J.R.; Müller, C.R. Effect of particle shape on domino wave propagation: A perspective from 3D, anisotropic discrete element simulations. *Granul. Matter* **2014**, *16*, 107–114. [[CrossRef](#)]
91. Lu, G.; Third, J.R.; Müller, C.R. Effect of wall rougheners on cross-sectional flow characteristics for non-spherical particles in a horizontal rotating cylinder. *Particuology* **2014**, *12*, 44–53. [[CrossRef](#)]
92. Williams, J.R.; O'Connor, R.M. Discrete element simulation and the contact problem. *Arch. Comput. Methods Eng.* **1999**, *6*, 279–304. [[CrossRef](#)]
93. Kačianauskas, R.; Tumonis, L.; Džiugys, A. Simulation of the normal impact of randomly shaped quasi-spherical particles. *Granul. Matter* **2014**, *16*, 339–347. [[CrossRef](#)]
94. Kruggel-Emden, H.; Rickelt, S.; Wirtz, S.; Scherer, V. A study on the validity of the multi-sphere discrete element method. *Powder Technol.* **2008**, *188*, 153–165. [[CrossRef](#)]
95. Kodam, M.; Bharadwaj, R.; Curtis, J.; Hancock, B.; Wassgren, C. Force model considerations for glued-sphere discrete element method simulations. *Chem. Eng. Sci.* **2009**, *64*, 3466–3475. [[CrossRef](#)]
96. Markauskas, D.; Kačianauskas, R.; Džiugys, A.; Navakas, R. Investigation of adequacy of multi-sphere approximation of elliptical particles for DEM simulations. *Granul. Matter* **2010**, *12*, 107–123. [[CrossRef](#)]

97. Galindo-Torres, S.A.; Pedroso, D.M. Molecular dynamics simulations of complex-shaped particles using Voronoi-based Spheropolyhedra. *Phys. Rev. E* **2010**, *81*, 061303. [[CrossRef](#)]
98. Lu, G.; Third, J.; Müller, C. Discrete element models for non-spherical particle systems: From theoretical developments to applications. *Chem. Eng. Sci.* **2015**, *127*, 425–465. [[CrossRef](#)]
99. Cooper, D.W. Random-sequential-packing simulations in three dimensions for spheres. *Phys. Rev. A* **1988**, *38*, 522–524. [[CrossRef](#)] [[PubMed](#)]
100. Visscher, W.M.; Bolsterli, M. Random packing of equal and unequal spheres in two and three dimensions. *Nature* **1972**, *239*, 504–507. [[CrossRef](#)]
101. Shashidhar, N.; Gopalakrishnan, K. Evaluating the aggregate structure in hot-mix asphalt using three-dimensional computer modeling and particle packing simulations. *Can. J. Civ. Eng.* **2006**, *33*, 945–954. [[CrossRef](#)]
102. Marek, M. Numerical modeling of random packed beds of various packing densities with a sequential deposition algorithm. In Proceedings of the 15th Conference on Computational Technologies in Engineering, Jora Wielka, Poland, 16–19 October 2018; p. 020015.
103. Yang, A.; Miller, C.; Turcoliver, L. Simulation of correlated and uncorrelated packing of random size spheres. *Phys. Rev. E* **1996**, *53*, 1516. [[CrossRef](#)]
104. Bezrukov, A.; Stoyan, D. Simulation and statistical analysis of random packings of ellipsoids. *Part. Part. Syst. Charact.* **2006**, *23*, 388–398. [[CrossRef](#)]
105. Liu, G.; Thompson, K.E. Influence of computational domain boundaries on internal structure in low-porosity sphere packings. *Powder Technol.* **2000**, *113*, 185–196. [[CrossRef](#)]
106. Hirsch, C.; Gaiselmann, G.; Schmidt, V. Asymptotic properties of collective-rearrangement algorithms. *ESAIM Probab. Stat.* **2015**, *19*, 236–250. [[CrossRef](#)]
107. Jodrey, W.S.; Tory, E.M. Computer simulation of close random packing of equal spheres. *Phys. Rev. A* **1985**, *32*, 2347–2351. [[CrossRef](#)] [[PubMed](#)]
108. Lubachevsky, B.D.; Stillinger, F.H. Geometric properties of random disk packings. *J. Stat. Phys.* **1990**, *60*, 561–583. [[CrossRef](#)]
109. Donev, A.; Cisse, I.; Sachs, D.; Variano, E.A.; Stillinger, F.H.; Connelly, R.; Torquato, S.; Chaikin, P.M. Improving the density of jammed disordered packings using ellipsoids. *Science* **2004**, *303*, 990–993. [[CrossRef](#)] [[PubMed](#)]
110. He, D.; Ekere, N.N.; Cai, L. Computer simulation of random packing of unequal particles. *Phys. Rev. E* **1999**, *60*, 7098–7104. [[CrossRef](#)]
111. Williams, S.R.; Philipse, A.P. Random packings of spheres and spherocylinders simulated by mechanical contraction. *Phys. Rev. E* **2003**, *67*, 051301. [[CrossRef](#)]
112. Trofimov, A.; Mishurova, T.; Lanzoni, L.; Radi, E.; Bruno, G.; Sevostianov, I. Microstructural analysis and mechanical properties of concrete reinforced with polymer short fibers. *Int. J. Eng. Sci.* **2018**, *133*, 210–218. [[CrossRef](#)]
113. Fritzen, F.; Böhlke, T. Periodic three-dimensional mesh generation for particle reinforced composites with application to metal matrix composites. *Int. J. Solids Struct.* **2011**, *48*, 706–718. [[CrossRef](#)]
114. Yang, Z.J.; Li, B.B.; Wu, J.Y. X-ray computed tomography images based phase-field modeling of mesoscopic failure in concrete. *Eng. Fract. Mech.* **2019**, *208*, 151–170. [[CrossRef](#)]
115. Schüler, T.; Jänicke, R.; Steeb, H. Nonlinear modeling and computational homogenization of asphalt concrete on the basis of XRCT scans. *Constr. Build. Mater.* **2016**, *109*, 96–108. [[CrossRef](#)]
116. Trawiński, W.; Tejchman, J.; Bobiński, J. A three-dimensional meso-scale modelling of concrete fracture, based on cohesive elements and X-ray μ CT images. *Eng. Fract. Mech.* **2018**, *189*, 27–50. [[CrossRef](#)]
117. Guo, F.q.; Zhang, H.; Yang, Z.j.; Huang, Y.j.; Withers, P.J. A spherical harmonic-random field coupled method for efficient reconstruction of CT-image based 3D aggregates with controllable multiscale morphology. *Comput. Methods Appl. Mech. Eng.* **2023**, *406*, 115901. [[CrossRef](#)]
118. Zhong, W.; Yu, A.; Liu, X.; Tong, Z.; Zhang, H. DEM/CFD-DEM modelling of non-spherical particulate systems: Theoretical developments and applications. *Powder Technol.* **2016**, *302*, 108–152. [[CrossRef](#)]

Disclaimer/Publisher’s Note: The statements, opinions and data contained in all publications are solely those of the individual author(s) and contributor(s) and not of MDPI and/or the editor(s). MDPI and/or the editor(s) disclaim responsibility for any injury to people or property resulting from any ideas, methods, instructions or products referred to in the content.